

Cardiac Flow Analysis Applied to Phase Contrast Magnetic Resonance Imaging of the Heart

KELVIN K. L. WONG,^{1,3} RICHARD M. KELSO,² STEPHEN G. WORTHLEY,³ PRASHANTHAN SANDERS,³
JAGANNATH MAZUMDAR,¹ and DEREK ABBOTT¹

¹Center for Biomedical Engineering and School of Electrical & Electronics Engineering, University of Adelaide, Adelaide, SA 5005, Australia; ²School of Mechanical Engineering, University of Adelaide, Adelaide, SA 5005, Australia; and ³Cardiovascular Research Centre and School of Medicine, University of Adelaide, Adelaide, SA 5005, Australia

(Received 14 July 2008; accepted 28 April 2009)

Abstract—Phase contrast magnetic resonance imaging is performed to produce flow fields of blood in the heart. The aim of this study is to demonstrate the state of change in swirling blood flow within cardiac chambers and to quantify it for clinical analysis. Velocity fields based on the projection of the three dimensional blood flow onto multiple planes are scanned. The flow patterns can be illustrated using streamlines and vector plots to show the blood dynamical behavior at every cardiac phase. Large-scale vortices can be observed in the heart chambers, and we have developed a technique for characterizing their locations and strength. From our results, we are able to acquire an indication of the changes in blood swirls over one cardiac cycle by using temporal vorticity fields of the cardiac flow. This can improve our understanding of blood dynamics within the heart that may have implications in blood circulation efficiency. The results presented in this paper can establish a set of reference data to compare with unusual flow patterns due to cardiac abnormalities. The calibration of other flow-imaging modalities can also be achieved using this well-established velocity-encoding standard.

Keywords—Velocity-encoding, Phase contrast magnetic resonance imaging, Vorticity, Cardiac flow analysis.

INTRODUCTION

Scanning and analysis of cardiac flow is a challenge due to the complexity of blood dynamics and myocardial motion. In a chamber of the heart, vortices are shown to exist as the result of the unique morphological changes of the cardiac chamber wall by using

flow-imaging techniques such as phase contrast magnetic resonance imaging. As the characteristics of our vorticity maps vary over a cardiac cycle, there is a need for a robust quantification method to analyze flow.

Important contributions to medical imaging and scientific knowledge are made in this study. We have devised a methodology to perform cardiac flow visualization and to be able to quantify flow dynamical changes over time. Measurement of vortex characteristics by means of calculating the vorticity and devising two-dimensional vortical flow maps can be performed. The technique relies on determining the vorticity statistics based on different time frames of one cardiac cycle. Our study has shown that a proper measurement of vorticity using the scanned flow field can characterize the location and strengths of large-scale vortices within a cardiac chamber. This approach, which is supported with qualitative flow visualization, can be utilized to explain cardiac flow behavior.

Velocity-encoded (VENC) phase contrast MRI allows three-dimensional MR velocity mapping based on the intrinsic sensitivity of MRI to flow, and enables the acquisition of spatially registered functional information simultaneously with morphological information.⁴¹ Three-dimensional MRI based velocity mapping operates by registering three separate flow-sensitive volumes in the x , y , and z orientations of the scan. The flow velocities may be computed by determining the shift of phase pertaining to the collection of imaged blood proton spins and reconstructing the flow vectors in advanced visualization packages. This concept has varying terminologies in literature, the most common being phase contrast MRI,⁴⁶ while some studies label it as phase-velocity MRI.⁵⁵ In general, such MRI based techniques form a class of approach known as magnetic resonance velocimetry (MRV), sometimes also called magnetic resonance image velocimetry (MRIV). These techniques have been very commonly used for

Address correspondence to Kelvin K. L. Wong, Center for Biomedical Engineering and School of Electrical & Electronics Engineering, University of Adelaide, Adelaide, SA 5005, Australia. Electronic mail: kwong@eleceng.adelaide.edu.au

Medical image processing software named Medflov, which is developed by Kelvin K. L. Wong, is used to produce the results displayed in this paper. The research-based version of this software system is utilized to provide cardiac flow visualization and analysis effectively.

producing visualization and investigation of flows even within non-organic structures.^{13,57}

The use of phase contrast magnetic resonance imaging (MRI) enables a good assessment of vortices that exist in the cardiac chamber. It is a non-invasive imaging technique that allows study of flow-related physiology and pathophysiology with good spatial and temporal resolutions. Vortical flow behavior has an effect on blood circulation.^{20,53} Previously, the study of vortices in the human heart has also been performed using velocity-encoded magnetic resonance (MR) imaging data.^{32,66,75} In particular, the study of vortices in the left atrium has been performed using three-dimensional phase contrast MRI.^{5,11,19} Therefore, this imaging modality is suggested for the flow imaging of cardiac chambers.

We develop planar flow maps of blood flow in the heart chambers and perform flow analysis using the tools described in this paper. The initial stage involves performing phase contrast MRI of the heart at short axis through the atria. The blood motion can be mapped in two dimension based on combination of the velocity signal maps pertaining to two directions. Vorticity in the flow is computed and mapping of the region of interest is performed. Finally flow statistics are computed globally for the flow region. We have identified two dominant vortices of opposite rotation in the right atrium for the initial time frames of one cardiac cycle. Based on another study, using slices from a different scan orientation, we map the influx of blood from the *vena cavae* into the right atrium and then through the mitral valve to the right ventricle. From subsequent studies, we have identified the presence of a large-scale vortex in the left atrium as well, and provide an indication of how a vortex in this heart chamber is diminishing as blood in this atrium flows into the left ventricle during the diastolic phase of the cardiac cycle.

Our paper is organized as follows: we give an introduction of the significance and implementation of phase contrast MRI. We also highlight the application of this technology for medical imaging of the heart, and particularly on flow visualization and analysis. The methodology section highlights the technical operation of the velocity-encoded phase contrast MRI. Experimental procedures are then stated and we introduce the building blocks and information flow charts that describe the cardiac flow measurement and visualization. The results section presents the velocity and vorticity flow maps of the heart. The flow phenomena in the human circulatory system are supported with physical interpretation of the blood and myocardial motion. Discussion of other existing technology that can perform flow measurement and visualization, as well as the clinical relevance of cardiac

flow analysis are detailed. Finally a conclusion is made based on the implications of the flow imaging framework in this study, and suggestions for future developments are mentioned.

MATERIALS AND METHODS

This section describes the concepts of phase contrast magnetic resonance imaging modalities and a measurement framework to calculate rotational flow or vorticity and quantify this parameter statistically in order to implement a new visualization system for flow patterns in cardiac chambers.

Phase Contrast MRI Velocimetry

Phase contrast MRI signals can be represented using intensity images.⁴² The intensity of each pixel corresponds to the blood velocity at the measured location. To quantify a velocity in one spatial dimension, at least two phase images must be taken for subtraction of flow-induced phase shift from background phases caused by susceptibility-induced inhomogeneities and coil sensitivity changes.² Blood velocity can be aliased to an artificially low value if it exceeds the maximum velocity encoded (VENC) by the flow sensitization gradients (see Fig. 1).

The phase contrast MRI technology is clinically attractive because it is able to provide quantitative information on blood flow without the need for contrast agent to be introduced into the human body. We present some images based on this MRI protocol in Fig. 2. The phase contrast images are graphical representations of the velocity components (x - and y -directions) maps. The figure shows the Foot–Head (F–H) and Anterior–Posterior (A–P) orientation scans.

Phase contrast MRI can be extended to three dimensions as well by combining an additional

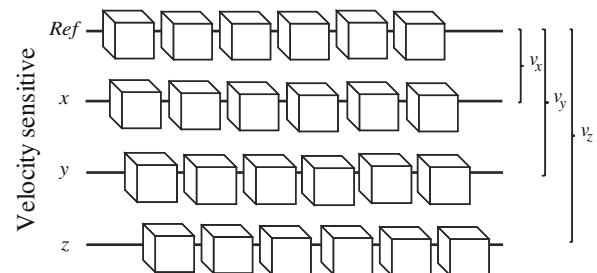


FIGURE 1. Phase contrast MRI velocimetry. Phase contrast MRI works on the concept that hydrogen nuclei from blood that has been exposed to magnetic fields accumulate a phase shift in spin that is proportional to the blood velocity in the x , y , and z directions. Velocities v_x , v_y , and v_z are functions of the subtractions of spin phases ϕ_x , ϕ_y , and ϕ_z of measured volumes with that of the reference phase ϕ_{Ref} .

PHASE CONTRAST MRI

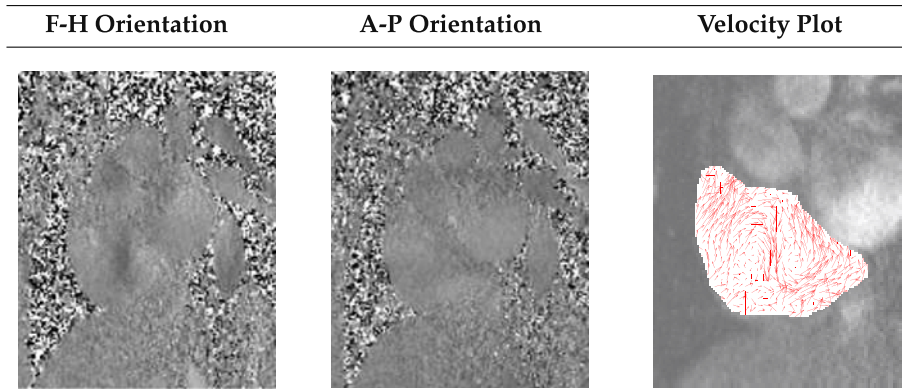


FIGURE 2. Phase contrast MRI of a cardiac chamber. Short axis scans pertaining to time frame indices $n_t = 11$ out of 25 frames in a cardiac cycle are presented. Scans based on two in-plane x - and y -directions, which pertains to the Foot-Head (F-H) and the Anterior-Posterior (A-P) orientations, respectively, are needed for velocity mapping. The intensity of the pixels in the image indicates the magnitude of the velocity component in the specified orientation. Combining two orthogonal velocity-encoded image maps can produce a two dimensional velocity flow field.

orientation, the through-plane image scans, to obtain the orthogonal velocity component map. Then, having the z -velocity component in addition to the in-plane flow components can be achievable. Although the extraction of the third velocity dimension can give a more accurate description of the flow scenario, the display of three-dimensional vectors in space is visually complicated and visualization may only be effective with the use of tools such as streamline tracing. Moreover, it is a challenge to incorporate anatomical information into the flow field by using planar magnetic resonance images insertion into a three-dimensional space that will partially occlude the flow patterns. For this reason, it may be more effective to view projections of velocity vectors onto a slice of interest through the cardiac flow field. The flow scenario with respect to the anatomy of the heart can be referenced by superimposing the two-dimensional cardiac flow onto the corresponding magnetic resonance image. Segmentation of the cardiac chamber will further define the boundary of blood motion and isolate the region of interest for flow analysis.⁷²

An electrocardiogram (ECG) can be used to synchronize image acquisition with cardiac motion to produce cine-magnetic resonance images.^{34,63} ECG gating can be performed prospectively or retrospectively.¹⁰ In prospective gating, the R-wave triggers image acquisitions in the cardiac cycle. Then, a trigger delay (or trigger window) provides an interval between the R-wave trigger and image acquisition.^{33,35} For retrospective gating,^{1,47,49,64} image acquisition occurs continuously along with an ECG tracing. Post-processing of images retrospectively using registered ECG tracing is performed. Cine-MRI of cardiac structures using ECG gating provides information on

cardiac flow and function. The first image acquired corresponds to the R-wave trigger (Fig. 3). Accurate QRS detection^{18,52,59,60,65} is crucial as it indicates reliable identification of the R-waves.

Vorticity Visualization System Implementation

A framework to measure flow within the cardiac structures has been devised based on the described techniques. The system is able to load magnetic resonance images and enables important functions such as segmentation of cardiac chambers, image reconstruction and flow visualization of blood, and statistical presentation of flow parameters. It can facilitate semi-automatic generation of case study reports of cardiac patients. The augmentation of visualization using the magnetic resonance image as a background gives a gauge of the location of blood volumes within the cardiac structure. Finally histogram generation and presentation of the vorticity, shear strain and normal strain magnitudes by the case study reports provides a concise indication of the characteristics of flow in the heart.

We describe the system configuration using processing components and their relevant data flow here. In this section, we construct the flow visualization system based on the theoretical concepts that we have covered in the previous sections. It is essential to establish a network of flow such that each of the procedure takes place in a systematic sequence to prepare the flow image results.

In order to understand the system of visualization, we quickly review the data processing pipeline in Fig. 4. The flow chart illustrates the blocks in an imaging and processing pipeline leading to the analysis

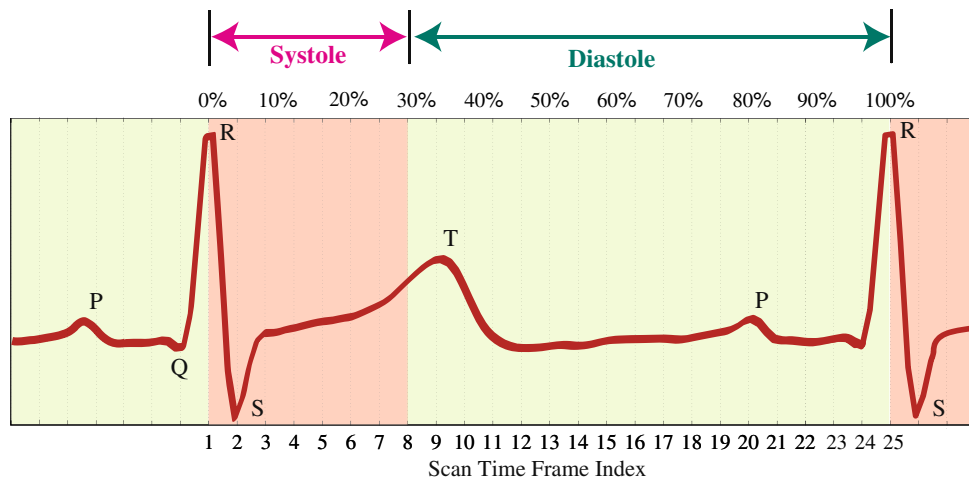


FIGURE 3. Cardiac events with relation to the electrocardiogram. The variation of a generic electrocardiogram (ECG) is correlated to the scan time frames of gated-MRI. The characteristic Q-, R-, S-, and T-waves are located at the elevations of the ECG trace. The triggering of image acquisition starts at the occurrence of the R-wave. For a temporal resolution of 25 time frames, the cardiac systole and diastole correspond to sets of frame indices that have ranges of 1 to 8 and 9 to 25 respectively.

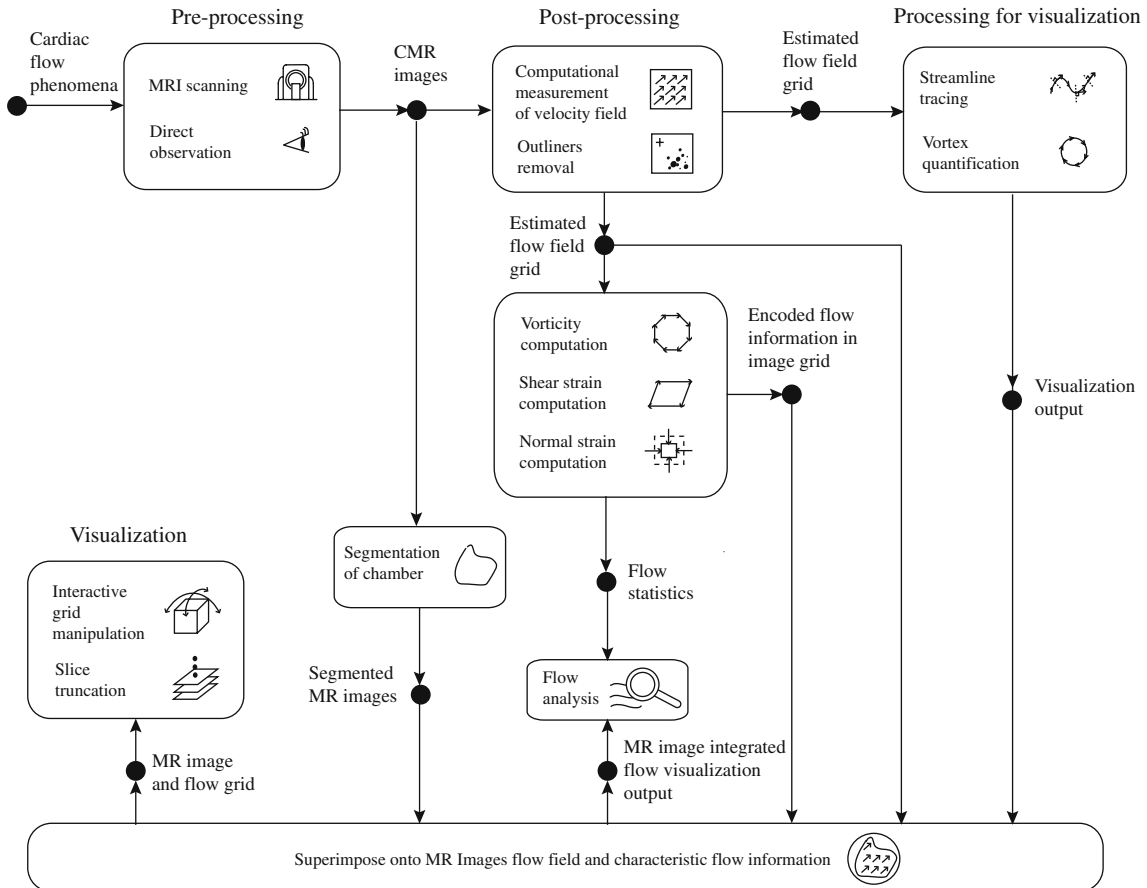


FIGURE 4. Cardiac vorticity visualization system. Visualization of flow can be based on a flow imaging framework. This system is a network of various modules that retrieves information from the previous stage of execution and continues until visualization is successful. The vorticity visualization system flow shows data processed by blocks depicting the magnetic resonance imaging, which provides data for generation of flow fields. The calculated flow data is fed into a flow characterization stage whereby other measures of the flow can be computed. These data are then used for flow characterization and field display based on streamline flow tracing, vector plot, and/or contour map.

of the visualization output. Beginning with the pre-processing stage, it can be seen that image retrieval from magnetic resonance scanning is carried out. Magnetic resonance imaging using the velocity-encoded phase contrast as well as standard steady-state free precession protocols can be carried out for the same subject in the scanner. Anatomical details based on the relevant scan slice can be observed. Following the cardiac magnetic resonance image retrieval stage, segmentation of the interested cardiac chamber is performed to isolate the derived fields within the boundary of flow regions from the endocardium.

The cardiac magnetic resonance data are also passed into the velocity grid reconstruction block whereby the flow field can be reconstructed based on deciphering of flow information from the images. For the velocity field, there exist inherent errors and an outlier detection program followed by vector interpolation is carried out to produce a complete smoothed velocity vector field. The output from this stage is the velocity field grid which can include up to one temporal and three spatial dimensions.

During the visualization stage, different resolutions of the vector plot can be implemented for optimal presentation and observation. Other visualization tools such as streamline tracing can be carried out for a more qualitative examination of the blood motion. Then the reconstructed velocity field grid are passed into the flow differential calculation stage, whereby each of the field grids is further processed to provide the strain rates or vorticity fields which can give more insight into the flow. The output will be encoded differential flow quantities in image form.

The processed visualization outputs can be combined in a graphical display platform in the subsequent stage and superimposed onto medical images that depict the anatomy of the heart. This allows positional and size referencing of the flow region against the cardiac structures in the heart. Consolidation of multiple cine-images at various slices can give a three-dimensional presentation of the flow images with interactive flow grid manipulation and slice truncation.

Features of interest in the flow study include magnitude, position, and numbers of counts of the vorticity and/or strain units spread throughout the flow map in the visualization display. The statistical compilation made in the final stage as well as the manipulated visualization outputs can contribute significantly to a more concise flow analysis.

In summary, the implemented system is based on stages of scanning, reconstruction, and computation that are constructed into a framework for the purpose of superior flow visualization and analysis of the heart. The derivation of flow quantities is based on the fluid mechanical properties of blood motion

which can be displayed using qualitative and quantitative outputs.

EXPERIMENTS

This section provides the scan information pertaining to each case study. It also describe the mathematical techniques for statistical analysis of flow and provides the framework for generating flow results qualitatively and quantitatively.

Case Study and MRI Scan Procedure

The velocity-encoded magnetic resonance imaging was performed using a Siemens Avanto, 1.5 Tesla, model-syngo MRB15 scanner with Numaris-4, Series No: 26406 software.

Case Study 1

Cine-magnetic resonance imaging was performed in short axis orientation through the atria. All images were acquired with retrospective gating and 25 phases or time frames (for time frame indices from $n_t = 1$ to 25) for each slice.

Using a normal and healthy male subject of age 22 years at the time of our case study, we examine the flow within the right atrium of his heart with a single set of scans pertaining to a slice at two-chamber short axis orientation. Our objective is to analyze the large-scale vortices that exist in the right atrium, and understand their development over the cardiac cycle. This allows us to identify the principal features of the flow in a normal heart versus an abnormal one.

Phase contrast magnetic resonance imaging is used to scan the normal subject. Acquisition parameters include: echo time TR = 47.1 ms, repetition time TE = 1.6 ms, field of view FOV = (298×340) mm² at a (134×256) pixel matrix. The in-plane resolution of 1.54 mm/pixel determined by the pixel spacing and the through-plane resolution is 6 mm based on the slice interval.

Scanning is performed at the section of the heart where the atria are positioned. This section is chosen such that the display of optimal cross-sectional area of the right atrium is enabled. A chamber size contains more data points to define the features of interest. The scan section is taken at a location shown in Fig. 5 whereby the scan is perpendicular to the axis joining the top of the heart to the apex through the septum. Multiple slices at this orientation are obtained throughout the atria. However, it is effective to base the velocity mapping on the right atrium of the heart using the scan sections that cut through the middle portion of atria. This corresponds to the maximum region of blood pool within the cardiac chamber in two

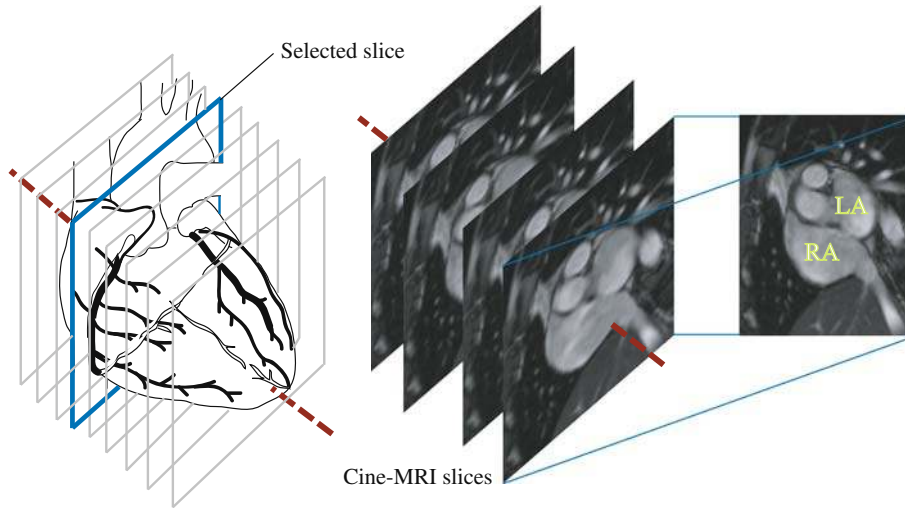


FIGURE 5. MRI scan through heart for case study 1. The scanning of the heart is taken at short axis and through two chambers, namely the left atrium (LA) and right atrium (RA). Therefore, this sectional view pertains to the two-chamber short axis scan. One planar scan is selected for flow examination of the right atrium as the case study.

dimensions. One slice, as shown in the schematic diagram of the heart, is selected for analysis in our study.

Case Study 2

Cine-magnetic resonance imaging was performed using a long axis orientation through the heart with displays of the atria and ventricles. All images were acquired with retrospective gating and 20 phases or time frames (for time frame indices from $n_t = 1$ to 20) for each slice.

We map the flow of the heart at a scan (two-chamber configuration) such that, based on two slices, the connections of the *vena cavae* to the right atrium as well as the pulmonary artery to the right ventricle are visible. For the first set of images, the influx of blood from the inferior *vena cavae* (at the bottom of the image) to the right atrium can be visualized. Blood is seen to move along the pulmonary artery (next to the aorta) away from the right ventricle almost simultaneously. This allows us to examine the effectiveness of the flow of blood from one region to the other. In a second set of scans (four-chamber configuration), we are able to observe the development of a left atrial vortex during diastolic phase of the cardiac cycle.

For the two-chamber view, phase contrast magnetic resonance image acquisition parameters include: echo time $TR = 46.85$ ms, repetition time $TE = 1.97$ ms, field of view $FOV = (234 \times 340)$ mm² at a (132×192) pixel matrix. For the four-chamber configuration, the image acquisition parameters are: echo time $TR = 54.45$ ms, repetition time $TE = 2.73$ ms, field of view $FOV = (318 \times 219)$ mm² at a (192×132) pixel matrix. The two sets of multi-slice scans at

two-chamber short axis and four-chamber long axis orientations have in-plane resolutions that are determined by the pixel spacing at 1.77 and 1.66 mm/pixel, respectively, whereas their through-plane resolution is based on the slice interval of 6 mm.

For this case study, multiple scans at a particular orientation (two-chamber short axis) are taken deliberately to assess the right atrium and its connective channels. The aim is to examine the nature of circulation pertaining to the *vena cavae*, the right atrium and right ventricle over the cardiac cycle. For this study, the imaging planes are tilted at an oblique angle with respect to the ones for case study 1 in order to capture these three anatomical entities. Multiple slices through the heart are scanned. These also correspond to the section that bisect the right atrium, where this chamber and the right ventricle, as well as the mitral valve in between them, can be imaged. Two out of the multiple scan slices are selected such that the inferior *vena cava* is visible in one image scan set, and the superior *vena cava* and pulmonary artery are visible in the other set.

Then, multiple scans at four-chamber long axis are performed to study the left and right atrial chambers and how their flow patterns develop over a cardiac cycle. For the right atrial flow, we aim to investigate the presence of swirling in the chamber. Based on a separate experiment, the flow relationship between the left atrium and ventricle is examined to understand the effect of atrial diastole on vortex development, followed by vortex breakup during its systolic phases. The slices that correspond to the middle portion of the left atrium and ventricle are selected. Figure 6 summarizes the scan orientations carried out for case study 2.

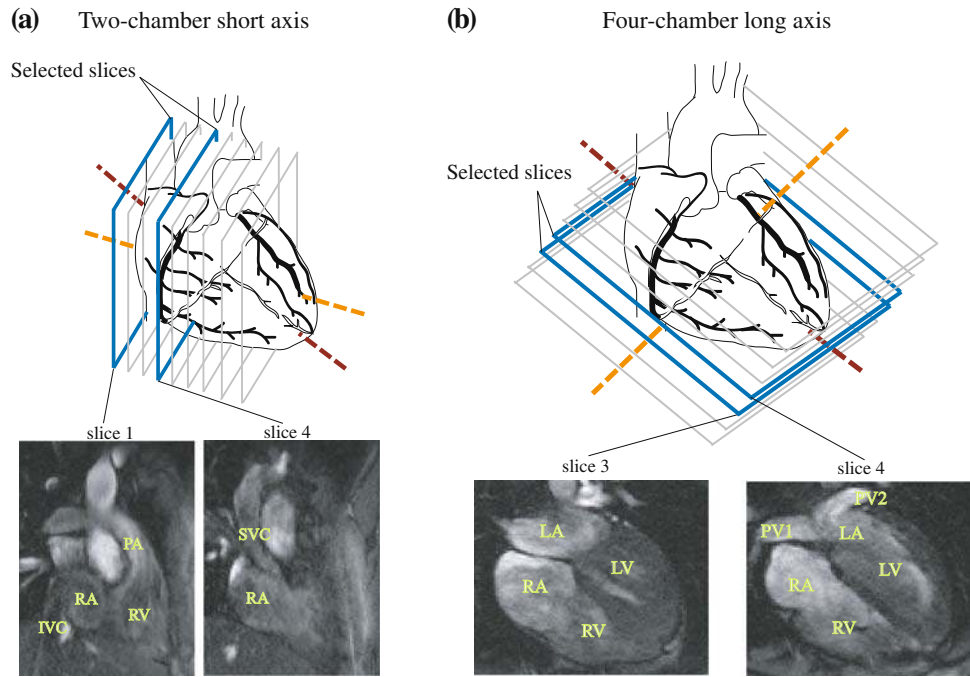


FIGURE 6. MRI scan through heart for case study 2. The scanning of the heart is performed using (a) two-chamber short axis to study the right atrium (RA), the right ventricle (RV), the inferior vena cava (IVC), the superior vena cava (SVC), and the pulmonary artery (PA). The image acquisition based on (b) four-chamber long axis is also carried out to examine flow in the right atrium (RA), the right ventricle (RV), the left atrium (LA), the left ventricle (LV), and two branches of the pulmonary vein (PV1 and PV2). Multiple slices at equal intervals are obtained. Only the appropriate slices, depending on the visibility of each cardiac anatomy, are chosen from each scan set for analysis.

Calibration Parameters

The magnetic resonance imaging parameters for phase contrast velocity encoding protocols are chosen for the flow field generation within the first and second case studies. Table 1 is created to summarize the scanning configuration. Note that the image display is a subset of the matrix scan image that is output by the magnetic resonance imaging scanner in order to show the region of interest specifically.

Flow Grid Representation

A dense velocity field (one velocity vector per pixel) is produced and a vector averaging based on a sampling window resolution of n by n pixels is carried out for the purpose of an aesthetical vector plot display within a segmented region of interest. We have set n to be 3 in our flow vector fields. The out-of-plane vorticity component is calculated from the in-plane velocity field using a finite element differential scheme.⁵⁶ A vorticity sampling mask size needs to be heristically set during the numerical derivation of the differential quantity. This sampling mask is experimentally determined based on a series of trial computations. It must be noted that the vorticity sampling window size determines the vorticity computation

based on a particular vortex scale.^{14–16} There is a need to obtain the optimal vorticity calculation and mapping, which produces vorticity values with the same range in each localized spatial group such that a vortex can be visually observed when the values are mapped onto a color scale. Typically, setting a large vorticity sampling size can remove noise fluctuations and obtain vorticity maps with minimum intra-class and maximum inter-class vorticity group values. However, this comes at the expense of over smoothing of vorticity values which causes data loss.

For processing of case study 1 scans, a vorticity sampling mask of size (21×21) pixels is set. The 21 pixels dimensional mask corresponds to a (32.34×32.34) mm² area. This mask is set to be relatively 7 to 8 times smaller than the displayed scan that is (184.80×231.00) mm². The vorticity sampling mask that is established for case study 2 is a (5×5) pixel frame that corresponds to (8.30×8.30) mm². The proportion of the scan display size to the sampling window size is approximately 24 times. It is relatively smaller since a smaller window region is to be mapped out of an overall smaller display image of (166.00×199.20) mm². Moreover, the spatial resolution of the first case study's scans is much higher and indicates the presence of larger-scale vortices with higher definition.

TABLE 1. Configuration of phase contrast magnetic resonance imaging.

Symbol	Quantity	Value	Units
Case study 2 scan set 1			
p_s	Pixel spacing	1.54	mm/pixel
t_s	Trigger time interval	29.43	ms
S	Slice thickness	6	mm
M_X	Matrix width	134	pixel
M_Y	Matrix height	256	pixel
X	Image width	120	pixel
Y	Image height	150	pixel
Case study 2 scan set 1			
p_s	Pixel spacing	1.77	mm/pixel
t_s	Trigger time interval	48.10	ms
S	Slice thickness	6	mm
M_X	Matrix width	132	pixel
M_Y	Matrix height	192	pixel
X	Image width	120	pixel
Y	Image height	150	pixel
Case study 2 scan set 2			
p_s	Pixel spacing	1.66	mm/pixel
t_s	Trigger time interval	47.35	ms
S	Slice thickness	6	mm
M_X	Matrix width	192	pixel
M_Y	Matrix height	132	pixel
X	Image width	100	pixel
Y	Image height	120	pixel

The scan properties of three sets of magnetic resonance imaging are presented here. Phase contrast MRI velocimetry is used to produce velocity flow fields. The vorticity flow maps can be determined from velocity information. These parameter values are used to calibrate these flow maps, as well as indicating the sampling vorticity mask size in metric units. Case study 1 scan set 1 pertains to the two-chamber short axis orientation which case study 2 scan sets 1 and 2 are based on the two-chamber and four-chamber long axis orientations, respectively.

p_s , Size of a pixel in metric unit; t_s , Duration of each time frame; S , Distance of slice interval; X , Width of matrix scan; Y , Height of matrix scan; X , Width of image display; Y , Height of image display.

Here, positive values signify counter-clockwise (CCW) rotation, whereas negative values represent clockwise (CW) motion of the blood. Therefore, the magnitudes of these values give an indication of the angular velocity and their polarity signifies the direction of the rotation. These may be represented by a color scale with maximum CCW and CW vorticity magnitudes corresponding to red and blue, respectively.

Parameters for Data Analysis

The histogram of a vorticity map with a size of n pixels in the range $\omega = [-L, L] \text{ s}^{-1}$, and with k number of bins (or histogram bars), is a discrete function $h(r_k) = N_k$. Here, r_k is the k th vorticity value and N_k is the number of pixels in the flow map having vorticity value r_k .²⁷ Based on this definition, the vorticity

histogram is a probability density function of occurrence of vorticity value r_k , whereby the sum of all components of a normalized histogram is equal to one.

Statistical quantification of the blood vorticity map in the right atrium is performed by translating all the scalar values into histogram format. Normalization is performed by standardising the total count of pixels within a segmented region of interest to create an equal integral area under the frequency plot of the flow map. Therefore the histogram can be numerically normalized by setting the sum of counts in all bins to an arbitrary value of 100 pixels (which we define as 100% counts achievable). The number of pixels N_k assigned to a bin results in capacity of p_k % of all pixels in a segmented atrial flow map, whereby

$$p_k(\%) = \frac{N_k}{N} \times 100\%. \quad (1)$$

The histograms pertaining to the vorticity field plots onto magnetic resonance images is produced for every phase of one cardiac cycle. A measure of the average vorticity value is computed by taking the mean $\bar{\omega}_\mu$ or median $\bar{\omega}_m$ of the frequency histograms that are generated from vorticity maps. Vorticity standard deviation σ with respect to μ are computed by considering the variation about the mean, and is denoted as σ_μ . Standard deviation about the median is denoted by σ_m .

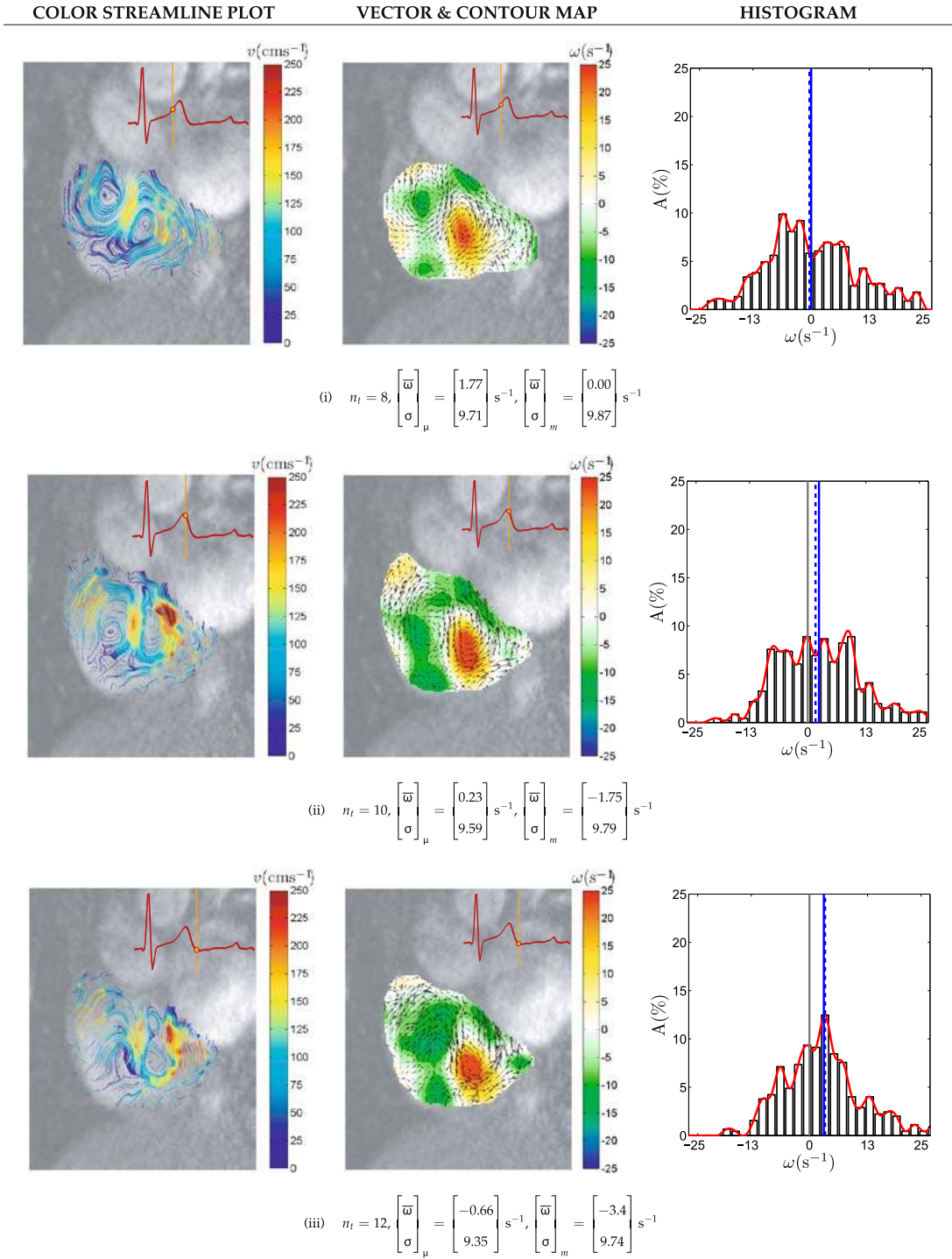
RESULTS

This section discusses the flow analysis based on results obtained from the magnetic resonance image velocity-mapping of the cardiac chambers and connective structures of the heart.

Flow in the Right Atrium

We observe the large-scale vortices that appear in the chamber of the heart and analyze their development and changes during selected time frame indices from $n_t = 8$ to 15. The variation of the blood flow field can be visually examined using streamlines, vector plots and vorticity contour maps as shown in Fig. 7. In addition, we superimpose the corresponding MR images onto these flow fields to give an indication of the location of the flow features with respect to the chamber walls. The time at which the image acquisition takes place can be referenced using an electrocardiogram (ECG) trace at the top right hand corner of every flow map. We use a generic ECG trace for each flow image. The peak of the trace represents the R-wave that triggers the commencement of image acquisition and terminates it at the end of the next cardiac cycle.^{18,52,59,60,65}

NORMAL SUBJECT



Time frame indices from 14 and 16 out of 25 frames in a cardiac cycle continues on the next page

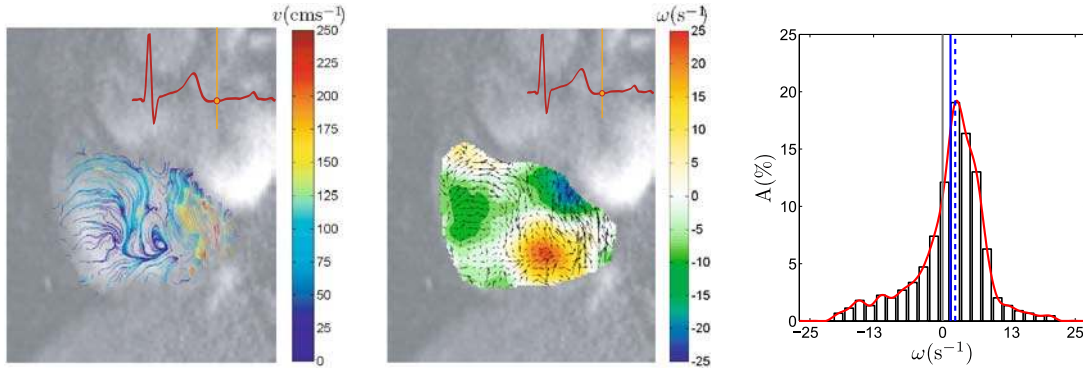
FIGURE 7. Flow visualization of normal right atrium. The visualization of flow in the right atrium of a normal subject is presented for investigation of the vortex behavior during the systolic and diastolic phases from time frame indices $n_t = 8$ to 16 of one cardiac cycle with 25 phases. The examination of flow patterns shows that the blood is swirling in both the clockwise and counter-clockwise directions simultaneously for some cardiac phases. Streamline plots are produced to illustrate the direction of blood in the chamber. Streamlines, with the color at every patch of the line indicates the magnitude of the velocity (in cm s^{-1}) and presents both the direction and speed of flow. A vector plot that is superimposed onto the vorticity contour map is also produced to indicate the location and strength of vortices. Each event of a cardiac cycle is indicated by a reference line on an echocardiogram (ECG) trace located on the top right hand corner of every image. This line updates its position as the time frame index increases.

NORMAL SUBJECT

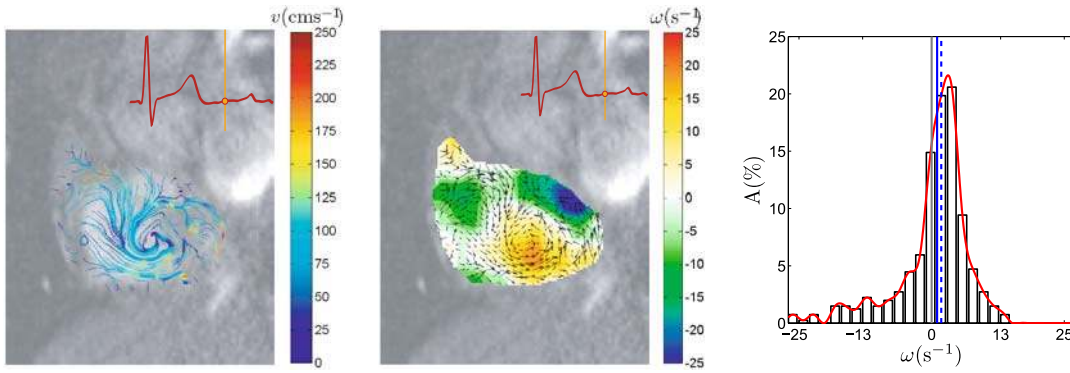
COLOR STREAMLINE PLOT

VECTOR & CONTOUR MAP

HISTOGRAM



$$(iv) \quad n_t = 14, \quad \begin{bmatrix} \bar{\omega} \\ \sigma \end{bmatrix}_\mu = \begin{bmatrix} -0.25 \\ 9.25 \end{bmatrix} \text{ s}^{-1}, \quad \begin{bmatrix} \bar{\omega} \\ \sigma \end{bmatrix}_m = \begin{bmatrix} -1.87 \\ 9.39 \end{bmatrix} \text{ s}^{-1}$$



$$(v) \quad n_t = 16, \quad \begin{bmatrix} \bar{\omega} \\ \sigma \end{bmatrix}_\mu = \begin{bmatrix} -0.56 \\ 10.62 \end{bmatrix} \text{ s}^{-1}, \quad \begin{bmatrix} \bar{\omega} \\ \sigma \end{bmatrix}_m = \begin{bmatrix} 0 \\ 10.64 \end{bmatrix} \text{ s}^{-1}$$

FIGURE 7. Continued.

Qualitative Examination of Right Atrial Flow

We present the flow results and analysis of the right atrium for the selected slice of the heart along the short axis orientation. Histograms are computed for each of these vorticity maps. Note that the mean and median of the histograms are denoted by $\bar{\omega}_\mu$ and $\bar{\omega}_m$, respectively. Standard deviations with respect to the mean and median are denoted as σ_μ and σ_m , respectively. The magnitude of vorticity using $\bar{\omega}_\mu$ and σ_μ may give an indication of the swirl in the right atrium. Based on our conventions, counter-clockwise and clockwise vorticity are represented in red and blue respectively on the contour map. Vortices in the atrium are shown to be dominantly counter-clockwise in rotation for most of the time frames based on the short axis view.

For a selected set of time frames based on one cardiac cycle, two large-scale vortices exist in the

chamber simultaneously. From Fig. 7, based on the streamline plots and vorticity contour maps, we are able to deduce that one counter-clockwise (CCW) vortex in the atrium exists along with a second clockwise (CW) vortex approximately to the upper-left of it.

Vortical flow based on the contour flow maps for the eight selected time frames of a cardiac cycle is characterized using the mean or median of all the map values. With reference to this case, the mean of the vorticity distribution $\bar{\omega}_\mu$ ranges from -0.66 to 2.13 s^{-1} while its median $\bar{\omega}_m$ ranges from -3.05 to 0.00 s^{-1} . Because of higher positive vorticity values generated by a stronger counter-clockwise vortex versus a weaker clockwise vortex, the distribution centroid is offset from the zero value. If the flow is dominantly a counter-clockwise rotation, the vorticity distribution is

typically bell-shaped and has a peak that lies in the positive domain of the distribution.

If there is an even number of vortices in the cardiac chamber of analysis, of which half of them pertain to a different direction of rotation, the magnitudes of $\bar{\omega}$ based on the mean or median cannot be used with reliability as a mode of analysis. This is due to the cancellation of positive and negative vorticity values for flow in all clockwise directions and counter-clockwise directions, respectively. Therefore, such global analysis is limited in terms of an accurate presentation of vorticity. In this case, visual observation and qualitative analysis will be more appropriate.

Another characteristic of the flow is the variance of the vorticity values, which can be based on its mean or median as the distribution centroid. The standard deviation of vorticity map σ that is based on the mean and median ranges from 7.13 to 12.64 s^{-1} and 7.53 to 12.81 s^{-1} , respectively. Vorticity images with high pixel color contrast result from maps with large standard deviations. There are a few reasons for a high σ , so it is of little value to use it for flow interpretation. Some possible reasons can be the presence of an odd number of equally strong vortices in the flow or numerous small vortices of different strengths, and the new vorticity that may be generated near the chamber wall regions.

In Fig. 8, we display the vorticity fields based on directional and absolute scalar map values. The absolute magnitude flow map will have a higher average vorticity as compared to the directional one whereas its standard deviation will remain the same. This can give an insight into the overall vorticity of the blood regardless of the rotation direction. The absolute vorticity means range from 5.67 to 9.99 s^{-1} . The corresponding median is 0 s^{-1} for almost all of the cardiac phases. Both distributions have standard deviations which ranges from 7.15 to 12.57 s^{-1} .

Vorticity Analysis of Right Atrial Flow

We observe qualitatively, based on the display of velocity and vorticity maps, two large-scale vortices of opposite rotations that appear in the right atrial flow. Note that each of them exists as a dominant vortex at some occasions throughout the cardiac cycle. We are able to indicate the relative strengths of the two vortices by plotting the directional means of vorticity maps with respect to cardiac time frames. If two vortices of equal strength but different polarities are developed in the region of analysis, the average of the vorticity field which is denoted by $\bar{\omega}$ is zero. When one vortex becomes stronger than the other one, the directional vorticity distribution centroid shifts to the positive or negative domain depending on the mean direction of rotation.

We take the ratio of directional vorticity mean to the absolute one as the normalized vorticity mean. As a vortex dominates the flow and the second vortex disappears completely, the normalized mean $\bar{\omega}_N$ approaches 1. When two equal and opposite vortices appear, $\bar{\omega}_N$ becomes 0. Intermediate levels of dominance can be indicated for $\bar{\omega}_N$ in the range of 0 to 1. The variation of $\bar{\omega}_N$ in Fig. 9 shows that a counter-clockwise vortex is present in the beginning. Then a vortex of opposite rotation grows in magnitude until it is slightly stronger than the first one. Eventually, this vortex diminishes and the initial dominant vortex occupies the chamber again. In conclusion, based on the statistics of these vorticity maps, we are able to describe the vortex development in a quantitative manner.

In the absence of other slices for the same analysis carried out here, there is a lack of evidence to show that the variation in vortex magnitude could be due to the changes in vortex locations over time. Therefore, to gain an accurate insight of the flow behavior in the cardiac chamber, we need to either examine the temporal variation of $\bar{\omega}_N$ for multiple slices in short axis orientations over the entire cardiac chamber, or a single long axis scan slice. The aim is to explore if the reduction in overall vortex strengths displayed by a vorticity map during subsequent time frames is the result of a vortex moving in the perpendicular direction of the slice, away from the sectional scan. Therefore, we generate flow maps of the right atrium and ventricle along the long axis orientation and examine the dynamics of blood in this view. It can be observed that in Fig. 10, based on selected time phases during atrial systole, there is a movement of blood from the right atrium into the ventricle and this may account for the motion of vortex away from the short axis plane of view towards the ventricle. It may be interesting to note that the linear or curvilinear translation of a vortex results in a spiral flow known as a helix.^{3,45,46}

Circulation of Blood Through the Right Atrium and Ventricle

Here, we present the flow visualization of blood which circulates in the right atrium, right ventricle, and connective veins and arteries to these chambers. Using the streamline trace diagrams, we are able to deduce the direction and speed of blood flow within the regions of interest. In Fig. 11a, we can observe the flow from superior *vena cava* at the onset of right atrial dilation. This event is seen to occur during the ventricular systolic phases. The pressures in the pulmonary arteries and veins are approximately 20 and 5 mmHg, respectively.^{6,8} Towards the end-systole, the flow slows down and a corresponding dilation of the

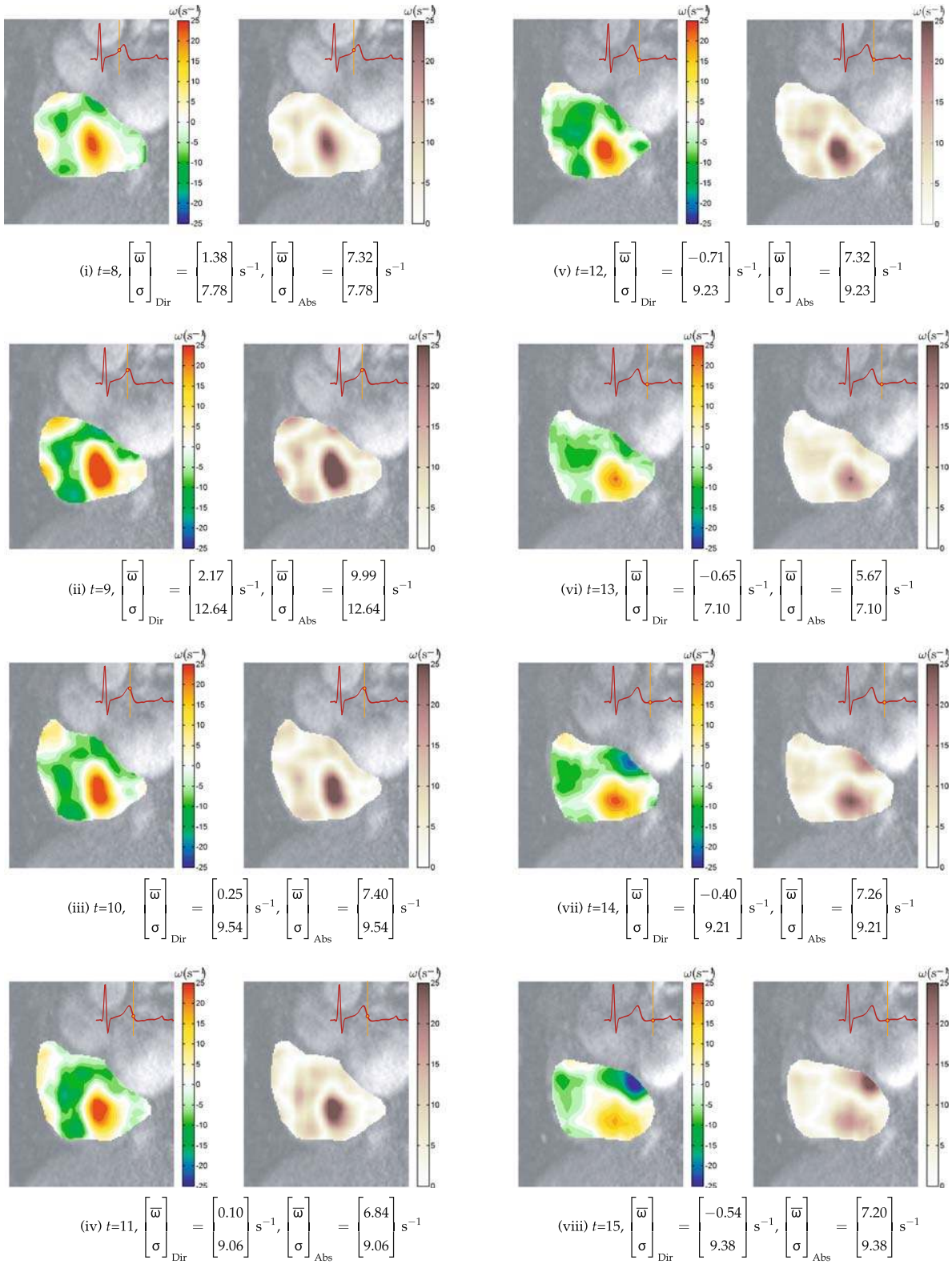


FIGURE 8. Flow quantification of normal right atrium. The statistics of each flow map based on mean and standard deviations for directional (Dir) and absolute (Abs) vorticity fields are provided for time frame indices $n_i = 8$ to 15 of one cardiac cycle with 25 frames. A directional field consists of polarized vorticity values that can depict clockwise or counter-clockwise fluid rotations. An absolute field displays vorticity magnitudes only.

Cardiac Flow Analysis

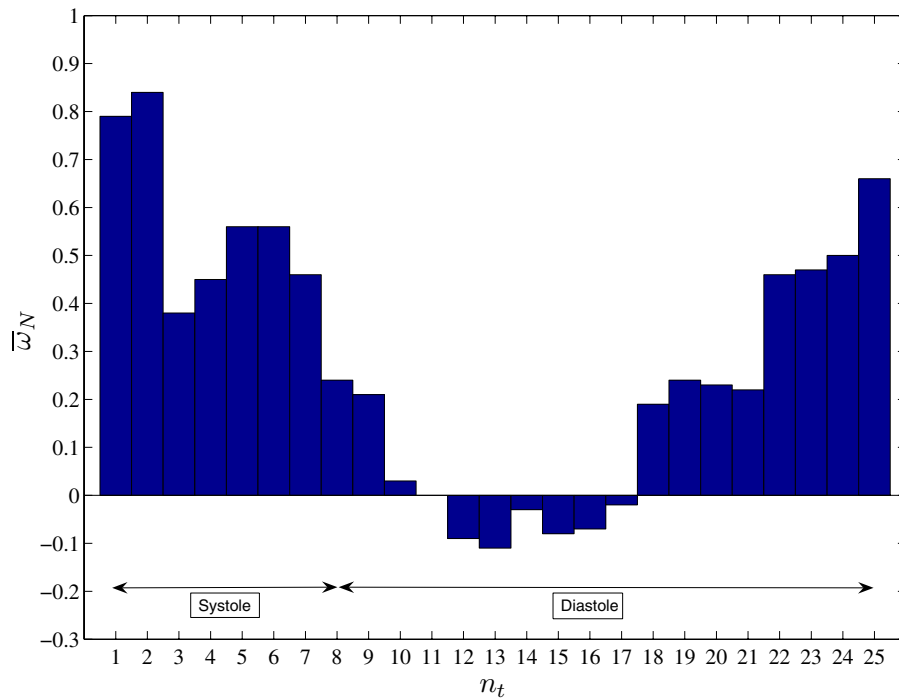


FIGURE 9. Chart of normalized vorticity mean based on a cardiac cycle. The relative strengths of vortices in a flow field can be indicated using the ratio of the directional mean to that of the absolute one. The plot of such normalized mean $\bar{\omega}_N$ with respect to time frame index n_t of a cardiac cycle demonstrates a smooth transition in positive vorticities losing dominance to the negative ones during time frame indices from $n_t = 10$ onwards and becoming higher in values again after $n_t = 18$.

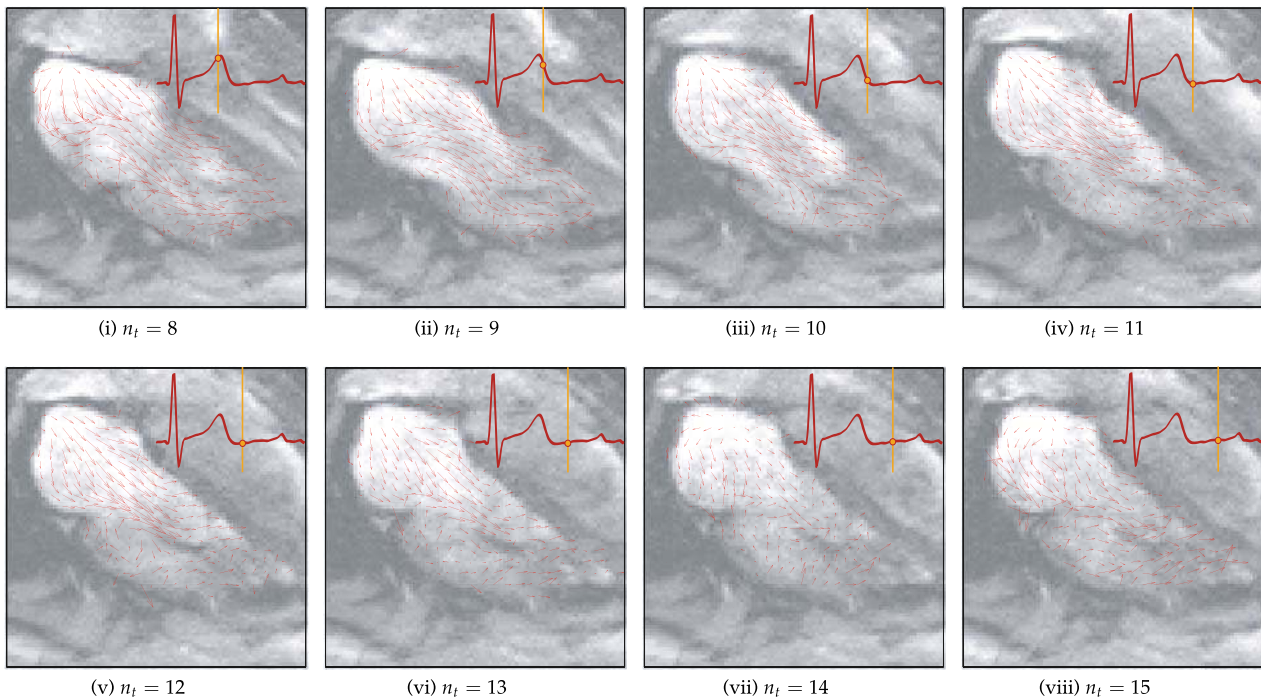


FIGURE 10. Qualitative visualization of flow in the right atrium and ventricle. The vector plots for selected time frame indices of $n_t = 8$ to 15 of a cardiac cycle with 20 frames demonstrates the movement of blood from the right atrium (RA) into the right ventricle (RV). There is no sign of large scale vortex formation in the RA during these atrial diastolic phases. The image set that is used here corresponds to slice three of the four-chamber long axis scan.

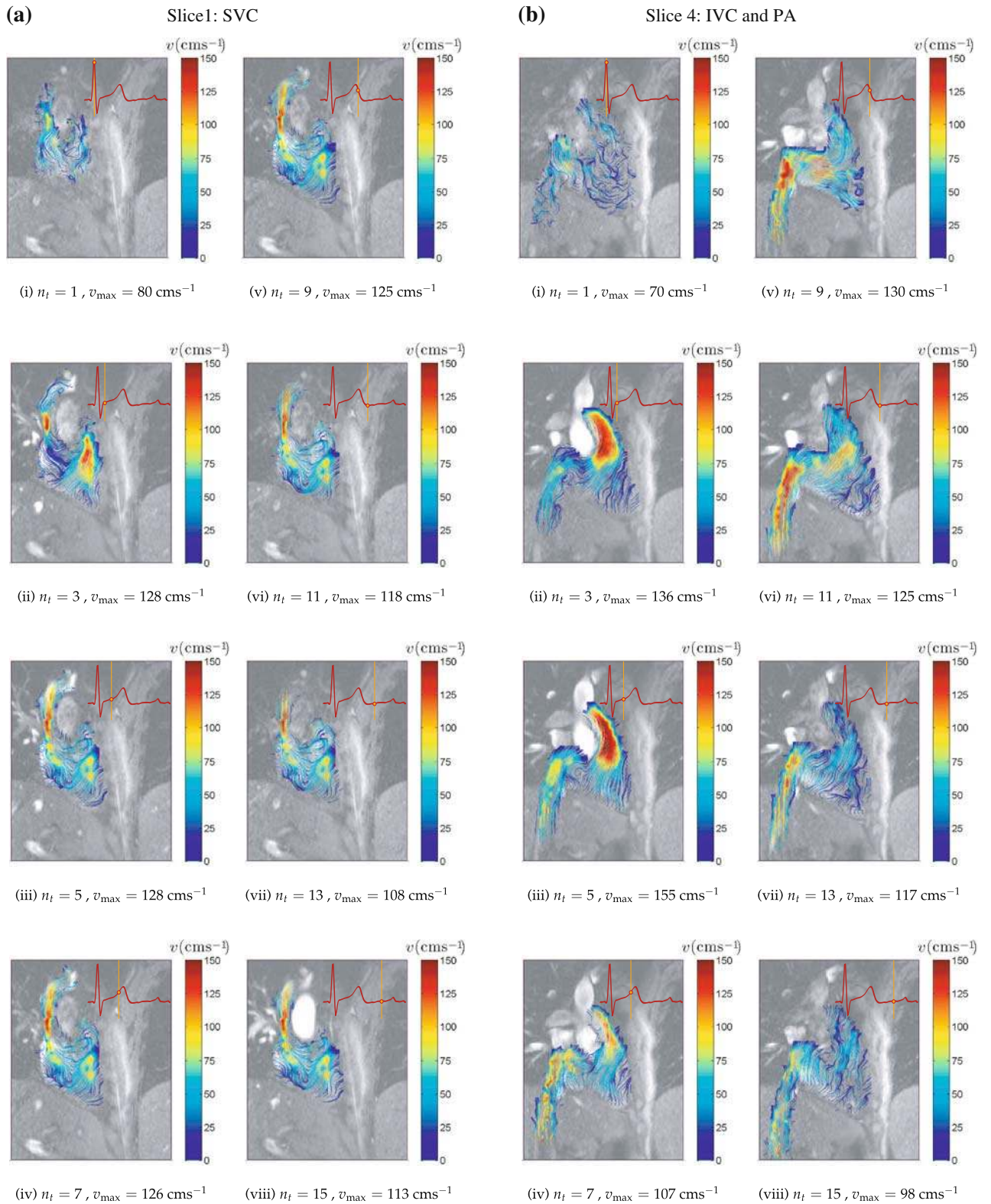


FIGURE 11. Qualitative visualization of right atrial flow circulation. The visualization of flow in the (a) inferior *vena cava* (IVC) and pulmonary artery (PA) and (b) superior *vena cava* (SVC) can be demonstrated by using streamline plots based on a cardiac cycle of 20 time frame indices. Flow is accelerated in the pulmonary artery during time frame indices from $n_t = 3$ onwards and its v_{\max} is 155 cm s^{-1} at $n_t = 5$. The flow in the inferior *vena cava* are shown to be accelerated during time frame indices $n_t = 9$ to 13 and has a maximum velocity v_{\max} of 128 cm s^{-1} at $n_t = 3$ and 5. These first and second events correspond to the systolic and diastolic phases, respectively.

right atrium induces the flow in the inferior and superior *vena cavae* to accelerate. We note that the blood streams entering the right atrium from these two channels interact to form a vortex.³²

With the opening of the atrioventricular valves during atrial systole, the blood surges into the relaxed ventricles, and then channels into the pulmonary artery.³² We note that there is an accelerated flow of blood in the pulmonary artery after the onset of the ventricular contraction (Fig. 11b). The ventricular contraction is triggered by the electrocardiographic R-wave which can lead to a rising pressure of up to 100 mmHg or greater.²² The absolute duration of a ventricular systole is defined as the time interval between the onset of the R-wave and the minimal ventricular volume on the volume–time activity curve.⁵⁴

The velocity of blood in the pulmonary artery is measured to reach up to 155 cm s^{-1} at some localized points in time. The average flow in the *vena cavae* are generally slower than the one in the artery, which typically ranges from approximately 0 to 80 cm s^{-1} . It is important to highlight that while a localized maximum velocity v_{max} can give an indication of the fastest blood flow at a specific region, it may not necessarily be higher than the ensemble average of the velocities in a region of interest. However, we observe that the maximum velocities measureable in our velocity maps also have a high range of velocities in the region, and so this quantity can be taken as an indicator of maximum global flow velocity here. The velocities measured are consistent with the typical range determined by pulsed Doppler examination.^{17,44}

We highlight that a heart may have different numbers and strengths of large-scale vortices in the right atrium. The flow imaging in our study shows that the right atrial vortex is predominantly counter-clockwise. This is due to the oblique alignment of the inferior and superior *vena cavae* in such a way that the flow presented from each vein introduces counter-clockwise angular momentum to the blood pool in the right atrium. The flow into the atrium increases during the atrial diastolic phases, thereby causing blood to gain this angular momentum and developing a counter-clockwise vortex.

Analysis of Vorticity in Left Atrial Flow

Streamline tracing of the velocity field pertaining to the atrium and ventricle on the left side of the heart is performed. The traces in Fig. 12 clearly demonstrate that a large-scale vortex exists in the left atrium during the cardiac systole. At this stage, no indication of swirling is observed in the ventricle. During the ventricular systole, pressure of the blood in the ventricular chamber causes the mitral and tricuspid valves to close

so that blood does not flow back into the left atrium.^{6,7} When the atrial systole takes place, the left atrium dilates. The counter-clockwise swirling in the left atrium is observed to be due to flow interaction from blood exiting out of the two branches of the pulmonary vein (PV1 and PV2) into the chamber. Due to the oblique alignment of the PV1 and PV2 flows, the interaction of these inflows from the two branches results in a diversion from their original courses of flow, and contributes to an angular momentum to the blood such that a counter-clockwise vortex is developed.³² This large-scale vortex is formed during the time frame indices $n_t = 7$ to 9. It moves away from the atrium during the atrial systolic phase as the atrioventricular valves open and the blood surges into the left ventricle.^{32,48} The velocity of the blood becomes maximum at time frame index $n_t = 10$ and can reach up to 175 cm s^{-1} at some local positions as it moves from the left atrium to the ventricle through the mitral valve. The surge jet leads to an asymmetric development of the initial vortex ring.⁵⁸ Flow decelerates slowly as the end stage of the atrial systole approaches. Some smaller-scale clockwise swirling is seen in the left ventricle subsequently during the onset of the cardiac systole (note $n_t = 11$ and 12). This observation is due to the formation of the vortex rings after the mitral flow.^{23,53}

DISCUSSION

We compare the characteristics and performance of phase contrast magnetic resonance imaging (PC-MRI) with an existing flow imaging modality that is based on ultrasound. The overall system evaluation of the flow-imaging and visualization framework is described and clinical relevance of this study is discussed.

Comparison of PC-MRI with Ultrasound Imaging Modality

Doppler ultrasound, as its name implies, is based on Doppler shift caused by blood scatter movement, and is a widely accepted technique to visualize blood flow patterns. Analysis of the flow field obtained by ultrasound methods enables useful results in cardiac diagnosis.²⁹ The Doppler ultrasound output is usually represented as a two-dimensional image.

Medical ultrasound works by generating high frequency electrical pulses and using piezoelectric elements of a transducer to convert them into mechanical vibrations. The emission of ultra-frequency sound and detection of sound waves from the resulting echoes is performed by transducers. After conversion into electrical signals, processing is carried out to decipher blood flow velocities.⁷¹ Ultrasound technology can be

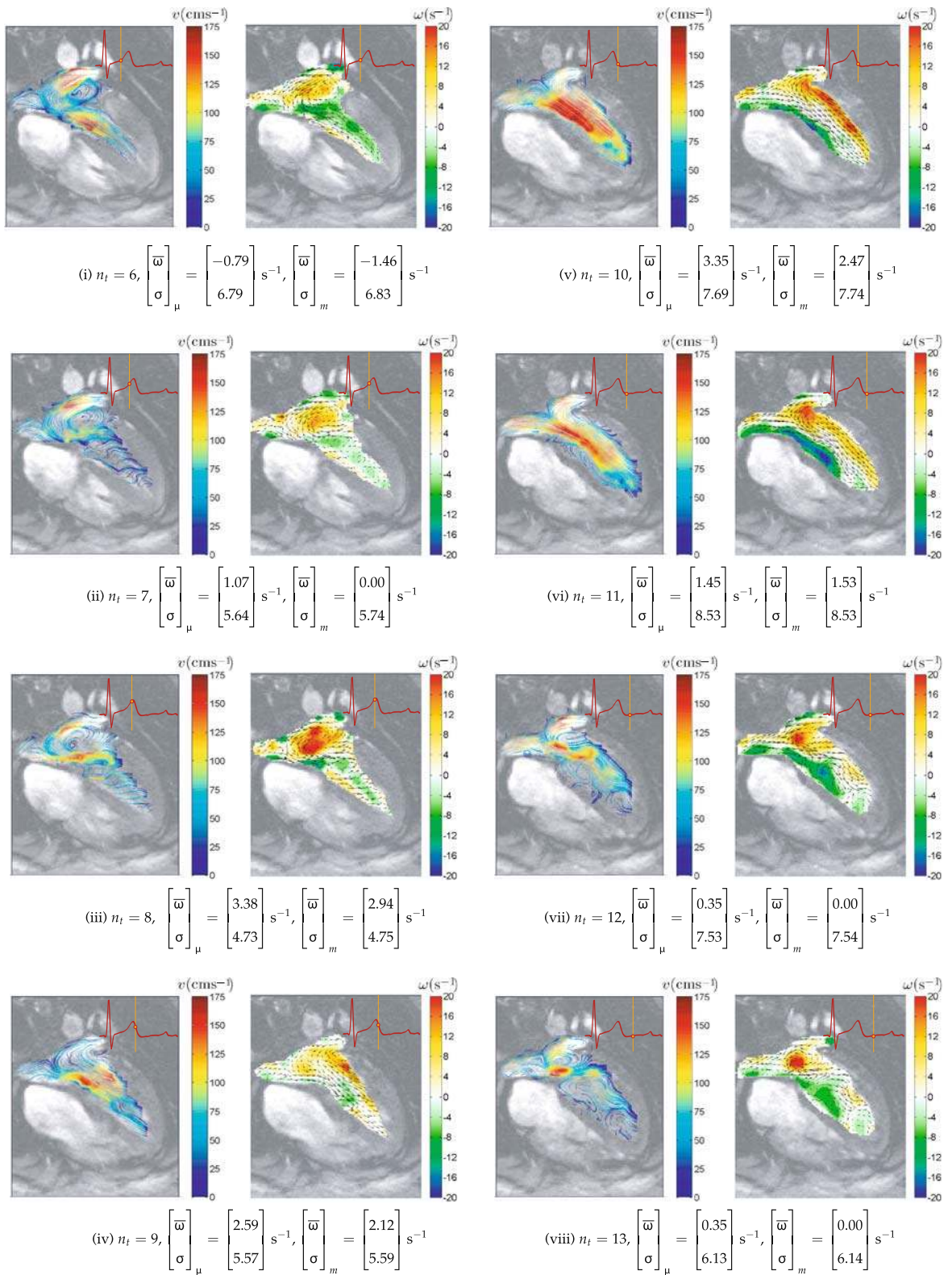


FIGURE 12. Flow quantification of normal left atrium and left ventricle. Streamline tracing and vorticity flow maps based on time frame indices $n_t = 6$ to 13 of one cardiac cycle with 20 frames. A counter-clockwise vortex is observed to form as flow through the two branches of the pulmonary vein (PV1 and PV2) into the left atrium (LA) from $n_t = 6$ to 8 gives the atrial blood an angular momentum. Subsequently, the swirling blood is forced into the left ventricle (LV) during the early stage of the cardiac diastole from $n_t = 9$ to 12.

used to diagnose cardiovascular diseases such as atrial septal defects⁶⁹ and also ambiguous calcific left main stenoses.⁶² Assessment of velocity waveforms of cardiac flow can be achieved using Doppler echocardiography.^{9,17,44}

Real-time blood motion imaging using color sonograms can be utilized. For this medical imaging modality, the speckle pattern from the blood flow signal is preserved, enhanced, and visualized.^{31,37} In this technique, a high frame rate is necessary for acquiring speckle pattern motion due to the rapid decorrelation of the speckle pattern from blood flow. In addition, good spatial resolution of the speckle pattern is essential.

A significant limitation of ultrasound imaging is that the Doppler shift is only sensitive to the velocity component in the orientation of the ultrasonic beam. However, clinical examination can be achieved with low cost and produces real-time flow visualization. In addition, ultrasound systems can be highly portable.⁶¹ This makes Doppler sonography more clinically attractive to use than magnetic resonance imaging (MRI). Despite these system advantages, a flow projection onto a plane for an accurate slice assessment of the cardiac flow is difficult to perform. Based on this aspect, it is inferior to velocity-coded MRI which can reconstruct accurate temporal flow grids of up to three spatial dimensions.²⁰

The superiority of magnetic resonance imaging over other imaging modalities is the capability of generating up to three-dimensional velocity profiles that can reflect the dynamics of blood flow more accurately and with quantifiable details. Apart from such localized measurements that can provide interactive visualization in cardiovascular flow,⁷⁴ phase contrast MRI has also been utilized in global flow measurements such as determination of flow volumes in arterial structures, and in particular, blood ejection volumes in the ascending aorta^{39,40,55} as well as arterial wall shear stress.^{50,51,68} It has been widely documented that phase contrast MRI is an established flow-imaging scheme for cardiovascular examination of human subjects and compares well with ultrasound technology.⁴⁰

Further development of phase contrast MRI to produce multi-slice cine images involves an electrocardiogram synchronized time-resolved framework to allow assessment of blood-flow characteristics with high spatial and temporal resolution of a cardiovascular region of interest.^{30,74} Sometimes there may be poor quality image registration due to poor respiratory control during scanning. Usually a ghosting artefact^{4,41,70} appears on the images. Other issues, such as limited signal-to-noise ratio control,⁴³ affect the imaging sensitivity of the scanning modality. Nevertheless, recent development of navigator-gated

time-resolved cine phase contrast MRI can control image distortion and ghosting effects due to the respiration of patients during image acquisition.⁴¹

System Performance

The full advantage of a flow imaging and visualization system lies in its integrated components, with focus on the data that each of them can generate, how the components are networked and the overall benefit that it can bring to clinical evaluation. Therefore, a successful application needs to be able to distinguish cardiac pathology from a normal heart part, such as pertaining to pre- and post-surgical intervention of cardiac structures, or to provide comparison of results from two different flow imaging modalities. It should also be able to provide a quantifiable indication of the difference. We develop a system that is able to achieve these aims.

Note that the computational reconstruction of flow based on intensity-based medical images is not immune to false intensity flow detection due to the different sources of magnetic field distortions during magnetic resonance imaging. For example, lung tissue occludes the heart, which results in a distortion of the static magnetic field,¹² can lead to detection of false blood signals. It is therefore crucial to use good quality images for computational reconstruction of the motion field in all our studies. In addition, image sizes have to be standardized when comparing flow before and after surgical intervention or when patient to patient comparisons are made.

Flow patterns are identified by making the flow visible using field vector plots. The streamline plot is a useful visual tool for tracing the motion of the fluid. An indication of the strength of a large-scale vortex can be given by using a color contour map. Reconstruction of a vorticity map as a color image allows examination of the flow.

Other flow visualization tools such as sphere glyphs, color ribbons, line segment glyphs, adjustable rakes, and barbell glyphs have been developed for use depending on the nature of the fluid flow.³⁶ However, it is beyond our scope to examine all of these techniques. Therefore, only streamlines, vector plots and vorticity color maps are used in various figures throughout this paper.

The construction of a flow grid using more than one set of orthogonal planes can provide a better indication of three-dimensional vortex flow structures. Nevertheless, the use of planar flow map slices provides a sufficient representation of the volumetric flow. At the preliminary stage, we can present flow analysis in the two-dimensional plane. The use of scans in one plane is sufficient to reveal flow behavior for characterization.

Clinical Relevance

The clinical relevance of intra-cardiac flow characteristics is critical. For example, pulmonary artery velocity measurements can evaluate cardiac conditions such as pulmonary hypertension, pulmonary stenosis and insufficiency, intracardiac shunts and congenital abnormalities.^{17,21} In addition, approximately 20% of cerebrovascular events have a cardiac source of embolis, and structural cardiac predictors (i.e., left atrium size and left ventricular function) are imperfect at identifying which patients are at risk. The ability to characterize intra-cardiac flow offers a new index that may provide risk predictors for certain individuals with embolic cardiovascular conditions. Clearly, further work is required to fully understand the normal range of intra-cardiac flow characteristics and to predict future embolic events.

The study of cardiac blood flow can provide qualitative insights into normal and pathological physiology as well as cardiovascular functions.^{24,25,32,41,55} Studies have shown that flow information can be used as an index of cardiac health.^{23,28,67,77} This motivates the need for cardiac flow measurement and visualization systems in practice. Flow visualization within the human heart augments the percipience and experience of cardiologists and can assist in the understanding of the genesis and progression of cardiac abnormalities. Quantitative prediction or diagnosis of cardiac failures is of importance for clinical applications. Medical organizations will be able to assess the degree of a cardiac abnormality in the heart so that appropriate medical action can be taken.

CONCLUSION

The use of velocity-encoded magnetic resonance imaging can reveal flow patterns within the human heart chambers, thereby opening up an understanding of the functional aspect of the heart. Extending this technique by the computation of vorticity maps can allow us to determine the characteristics of the vortices to an extent. The use of statistics and histograms of vorticity maps can aid in the analysis of the blood circulation at various time frames of a cardiac cycle.

The velocity fields are based on the phase contrast magnetic resonance images that the scanner provides. The flow can be calibrated and streamline traces of the field can provide a clear visualization of blood movement with information such as the speed and direction. Vorticity is generated from the motion vector field to display the location and strength of vorticities in

the flow. We illustrate the usefulness of these qualitative information displays in this paper.

The study has shown that swirling flow is present in the right and left atria of the heart. However, such movements vary over time and are influenced by the movement of the myocardium. Using scans of the right atrium in the short axis orientation, we determine the characteristics of the vortices within the chamber. Based on long axis scans, we also observe that blood is drawn into the heart chamber at different events of the cardiac cycle. Finally, from the four-chamber long axis view, we produce visualization of left atrial vortex using streamline tracing and vorticity mapping. The evolution of the vortex can be analyzed qualitatively and quantitatively.

The velocity-mapping framework that we develop can be applied to assess flow in various heart chambers and circulation in the veins and arteries. A benefit of our framework is the coupling of flow visualization with quantifiable data that may give an indication of the vorticity changes in the cardiac flow. The flow quantification methods in this work is new, and further studies based on a larger population group and other portions of the heart or circulation can be performed in future to validate the cardiac flow analytical framework. The results may also be used to validate computational fluid dynamics simulations^{26,38,76} and techniques such as magnetic resonance fluid motion tracking⁷³ can be verified in terms of accuracy based on velocity-encoded flow maps. In addition, we can try to develop three-dimensional streamline visualization of the blood flow which can eliminate the use of multiple slices to cover the flow details adequately. Although we understand that complicated flow patterns may clutter the three-dimensional flow visualization and cause qualitative analysis to be difficult, it may be worthwhile performing flow modeling using interactive manipulation of the flow field display to gain a clearer insight of the flow.

ACKNOWLEDGMENT

The authors thank the Royal Adelaide Hospital for the supply of magnetic resonance images, and to Payman Molae for his assistance in scanning the subject used in this research. Special thanks are also extended to Fangli Xiong from Nanyang Technological University (Singapore) and the reviewers of this paper. Their comments and suggestions, which have made the paper more meaningful and interesting, are gratefully acknowledged.

REFERENCES

- ¹Achenbach, S., S. Ulzheimer, U. Baum, M. Kachelriess, D. Ropers, T. Giesler, W. Bautz, W. G. Daniel, W. A. Kalender, and W. Moshage. Noninvasive coronary angiography by retrospectively ECG-gated multislice spiral CT. *Circulation* 102:2823, 2000.
- ²Baltes, C., S. Kozerke, M. S. Hansen, K. P. Pruessmann, J. Tsao, and P. Boesiger. Accelerating cine phase-contrast flow measurements using k-t BLAST and k-t SENSE. *Magnet. Reson. Med.* 54(6):1430–1438, 2005.
- ³Bogren, H. G., and M. H. Buonocore. 4D magnetic resonance velocity mapping of blood flow patterns in the aorta in young vs. elderly normal subjects. *J. Magn. Reson. Imag.* 10(5):861–869, 1999.
- ⁴Bogren, H. G., M. H. Buonocore, and R. J. Valente. Four-dimensional magnetic resonance velocity mapping of blood flow patterns in the aorta in patients with atherosclerotic coronary artery disease compared to age-matched normal subjects. *J. Magn. Reson. Imag.* 19:417–427, 2004.
- ⁵Brandt, E., T. Ebberts, L. Wigström, J. Engvall, and M. Karlsson. Automatic detection of vortical flow patterns from three-dimensional phase contrast MRI. *Proc. Int. Soc. Magnet. Reson. Med.* 9:1838, 2001.
- ⁶Chandran, K. B. Cardiovascular Biomechanics. New York University Biomedical Engineering Series, New York University Press, 1992.
- ⁷Chandran, K. B., A. Wahle, S. C. Vigmostad, M. E. Olszewski, J. D. Rossen, and M. Sonka. Coronary arteries: imaging, reconstruction, and fluid dynamic analysis. *Crit. Rev. Biomed. Eng.* 34(1):23–103, 2006.
- ⁸Chandran, K. P., A. P. Yoganathan, and S. E. Rittgers. Biofluid Mechanics: The Human Circulation. CRC Press, Taylor & Francis Group, 2006.
- ⁹Chaoui, R., F. Taddei, G. Rizzo, C. Bast, F. Lenz, and R. Bollmann. Doppler echocardiography of the main stems of the pulmonary arteries in the normal human fetus. *Ultrasound Obst. Gyn.* 11(3):173–179, 2002.
- ¹⁰Du, Y. P., E. R. McVeigh, D. A. Bluemke, H. A. Silber, and T. K. F. Foo. A comparison of prospective and retrospective respiratory navigator gating in 3D MR coronary angiography. *Int. J. Cardiovasc. Imag.* 17(4):287–294, 2001.
- ¹¹Ebberts, T., L. Wigström, A. F. Bolger, B. Wranne, and M. Karlsson. Noninvasive measurement of time-varying three-dimensional relative pressure fields within the human heart. *J. Biomech. Eng.* 124(3):288–293, 2002.
- ¹²Edelman, R. R. Contrast-enhanced MR imaging of the heart: overview of the literature. *Radiology* 232:653–668, 2004.
- ¹³Elkins, C. J., M. Markl, A. Iyengar, R. Wicker, and J. Eaton. Full field velocity and temperature measurements using magnetic resonance imaging in turbulent complex internal flows. *Int. J. Heat Fluid Flow* 25:702–710, 2004.
- ¹⁴Etebari, A., and P. P. Vlachos. Improvements on the accuracy of derivative estimation from DPIV velocity measurements. *Exp. Fluids* 39(6):1040–1050, 2005.
- ¹⁵Ferziger, J. H., and M. Peric. Computational Methods for Fluid Dynamics, 3rd edn. Springer, 2001, Number ISBN: 3540420746.
- ¹⁶Foucaut, J. M., and M. Stanislas. Some considerations on the accuracy and frequency response of some derivative filters applied to particle image velocimetry vector fields. *Meas. Sci. Technol.* 13:1058–1071, 2002.
- ¹⁷Freedom, R. M., S.-J. Yoo, H. Mikailian, and W. Williams. The Natural and Modified History of Congenital Heart Disease. Blackwell Publishing, 2003.
- ¹⁸Friesen, G. M., T. C. Jaqnnett, M. A. Jadallah, S. L. Yates, S. R. Quint, and H. T. Nagle. A comparison of the noise sensitivity of nine QRS detection algorithms. *IEEE Trans. Bio-Med. Eng.* 37:85, 1990.
- ¹⁹Fyrenius, A., T. Ebberts, L. Wigström, M. Karlsson, B. Wranne, A. F. Bolger, and J. Engvall. Left atrial vortices studied with 3D phase contrast MRI. *Clin. Physiol. Funct. Imag.* 19(3):195, 1999.
- ²⁰Fyrenius, A., L. Wigström, T. Ebberts, M. Karlsson, J. Engvall, and A. F. Bolger. Three dimensional flow in the human left atrium. *Heart* 86:448–455, 2001.
- ²¹Gardin, J. M., H. W. Sung, A. P. Yoganathan, J. Ball, S. McMillan, and W. L. Henry. Doppler flow velocity mapping in an in vitro model of the normal pulmonary artery. *J. Am. Coll. Cardiol.* 12:1366–1376, 1988.
- ²²Gertsch, M., and C. P. Cannon. The ECG: A Two-Step Approach to Diagnosis. Springer, 2003.
- ²³Gharib, M., E. Rambod, A. Kheradvar, D. J. Sahn, and J. O. Dabiri. A global index for heart failure based on optimal vortex formation in the left ventricle. *Proc. Natl. Acad. Sci. USA (PNAS)* 103(16):6305–6308, 2006.
- ²⁴Ghista, N. D. Applied Biomedical Engineering Mechanics. CRC Press, 2008.
- ²⁵Ghista, N. D., and E. Y.-K. Ng. Cardiac Perfusion and Pumping Engineering (Clinically-Oriented Biomedical Engineering). World Scientific Publishing Company, 2007.
- ²⁶Glor, F. P., J. J. M. Westenberg, J. Vierendeels, M. Danilouchkine, and P. Verdonck. Validation of the coupling of magnetic resonance imaging velocity measurements with computational fluid dynamics in a U bend. *Artif. Organs* 26(7):622–635, 2008.
- ²⁷Gonzalez, R. C., and R. E. Woods. Digital Image Processing, 2nd edn. New Jersey, USA: Prentice-Hall, Inc., 2002.
- ²⁸Hasegawa, H., W. C. Little, M. Ohno, S. Brucks, A. Morimoto, H.-J. Cheng, and C.-P. Cheng. Diastolic mitral annular velocity during the development of heart failure. *J. Am. Coll. Cardiol.* 41:1590–1597, 2003.
- ²⁹Hatle, L., and B. Angelsen. Doppler Ultrasound in Cardiology: Physical Principles and Clinical Applications. 2nd ed. Philadelphia: Lea and Febiger, 1982.
- ³⁰Herold, V., P. Mörchel, C. Faber, E. Rommel, A. Haase, and P. M. Jakob. In vivo quantitative three-dimensional motion mapping of the murine myocardium with PC-MRI at 17.6 T. *Magn. Reson. Med.* 55:1058–1064, 2006.
- ³¹Kasai, C., K. Namekawa, A. Koyano, and R. Omoto. Real-time two-dimensional blood flow imaging using an autocorrelation technique. *IEEE Trans. Sonics Ultrasonics* 32(3):458–464, 1985.
- ³²Kilner, P. J., G.-Z. Yang, A. J. Wilkes, R. H. Mohiaddin, D. N. Firmin, and M. H. Yacoub. Asymmetric redirection of flow through the heart. *Nat. Med.* 404:759–761, 2000.
- ³³Koktzoglou, I., A. Kirpalani, T. J. Carroll, D. Li, and J. C. Carr. Dark-blood MRI of the thoracic aorta with 3D diffusion-prepared steady-state free precession: initial clinical evaluation. *Am. Roentgen Ray Soc.* 189:966–972, 2007.
- ³⁴Larson, A. C., R. D. White, G. Laub, E. R. McVeigh, D. Li, and O. P. Simonetti. Self-gated cardiac cine MRI. *Magnet. Reson. Med.* 51(1):93–102, 2004.
- ³⁵Ley, S., J. Ley-Zaporozhan, K. Kreitner, S. Iliyushenko, M. Puderbach, W. Hosch, H. Wenz, J. Schenk, and H. Kauczor. MR flow measurements for assessment of the pulmonary, systemic and bronchosystemic circulation: impact of different ECG gating methods and breathing schema. *Eur. J. Radiol.* 61(1):124–129, 2007.

- ³⁶Lodha, S. K., A. Pang, R. E. Sheehan, and C. M. Wittenbrink. UFLOW: Visualizing uncertainty in fluid flow. In: Seventh IEEE Visualization 1996 (VIS '96), pp. 249–254, 1996.
- ³⁷Loevstakken, L., S. Bjaerum, D. Martens, and H. Torp. Real-time blood motion imaging v a 2D blood flow visualization technique. *IEEE Ultrasonics Symp.* 1:602–605, 2004.
- ³⁸Long, Q., X. Y. Xu, U. Köhler, M. B. Robertson, I. Marshall, and P. Hoskins. Quantitative comparison of CFD predicted and MRI measured velocity fields in a carotid bifurcation phantom. *Biorheology* 39(3–4):467–474, 2002.
- ³⁹Lotz, J., C. Meier, A. Leppert, and M. Galanski. Cardiovascular flow measurement with phase-contrast MR imaging: basic facts and implementation. *Radiographics* 22:651–671, 2002.
- ⁴⁰Maier, S. E., D. Meier, P. Boesiger, U. T. Moser, and A. Vieli. Human abdominal aorta: comparative measurements of blood flow with MR imaging and multigated Doppler US. *Radiology* 171:487–492, 1989.
- ⁴¹Mark, M., A. Harloff, T. A. Bley, M. Zaitsev, B. Jung, E. Weigang, M. Langer, J. Hennig, and A. Frydrychowicz. Time-resolved 3D MR velocity mapping at 3T: improved navigator-gated assessment of vascular anatomy and blood flow. *J. Magn. Reson. Imag.* 25:824–831, 2007.
- ⁴²Markl, M., F. P. Chan, M. T. Alley, K. L. Wedding, M. T. Draney, C. J. Elkins, D. W. Parker, R. Wicker, C. A. Taylor, R. J. Herfkens, and N. J. Pelc. Time-resolved three-dimensional phase-contrast MRI. *J. Magn. Reson. Imag.* 17:499–506, 2003.
- ⁴³Markl, M., M. T. Draney, M. D. Hope, J. M. Levin, F. P. Chan, M. T. Alley, N. J. Pelc, and R. J. Herfkens. Time-resolved 3-dimensional velocity mapping in the thoracic aorta: visualization of 3-directional blood flow patterns in healthy volunteers and patients. *J. Comput. Assist. Tomogr.* 28:459–468, 2004.
- ⁴⁴Mielke, G., and N. Benda. Blood flow velocity waveforms of the fetal pulmonary artery and the ductus arteriosus: reference ranges from 13 weeks to term. *Ultrasound Obst. Gyn.* 15(3):213–218, 2002.
- ⁴⁵Morbiducci, U., R. Ponzini, M. Grigioni, and A. Redaelli. Helical flow as fluid dynamic signature for atherogenesis risk in aortocoronary bypass. a numeric study. *J. Biomech.* 40(3):519–534, 2007.
- ⁴⁶Morbiducci, U., R. Ponzini, G. Rizzo, M. Cadioli, A. Esposito, F. De Cobelli, A. Del Maschio, F. M. Montevicchi, and A. Redaelli. In vivo quantification of helical blood flow in human aorta by time-resolved three-dimensional cine phase contrast magnetic resonance imaging. *Ann. Biomed. Eng.* 37(3):516–531, 2009.
- ⁴⁷Morgan-Hughes, G. J., A. J. Marshall, and C. Roobottom. Morphologic assessment of patent ductus arteriosus in adults using retrospectively ECG-gated multidetector CT. *Am. J. Roentgenol.* 181:749–754, 2003.
- ⁴⁸Narula, J., M. A. Vannan, and A. N. DeMaria. Of that waltz in my heart. *J. Am. Coll. Cardiol.* 49:917–920, 2007.
- ⁴⁹Nijm, G. M., A. V. Sahakian, S. Swiryn, J. C. Carr, J. J. Sheehan, and A. C. Larson. Comparison of self-gated cine MRI retrospective cardiac synchronization algorithms. *J. Magn. Reson. Imag.* 28(3):767–772, 2008.
- ⁵⁰Oyre, S., E. M. Pedersen, S. Ringgaard, P. Boesiger, and W. P. Paaske. In vivo wall shear stress measured by magnetic resonance velocity mapping in the normal human abdominal aorta. *Eur. J. Vasc. Endovasc. Surg.* 13:263–271, 1997.
- ⁵¹Oyre, S., S. Ringgaard, S. Kozerke, W. P. Paaske, M. Erlandsen, P. Boesiger, and E. M. Pedersen. Accurate noninvasive quantitation of blood flow, cross-sectional lumen vessel area and wall shear stress by three-dimensional paraboloid modeling of magnetic resonance imaging velocity data. *J. Am. Coll. Cardiol.* 32:128–134, 1998.
- ⁵²Pan, J., and W. J. Tompkins. A real-time QRS detection algorithm. *IEEE Trans. Bio-Med. Eng.* 32(3):230–236, 1985.
- ⁵³Pierrakos, O., and P. P. Vlachos. The effect of vortex formation on left ventricular filling and mitral valve efficiency. *J. Biomech. Eng.-Trans. ASME* 128(4):527–539, 2006.
- ⁵⁴Plehn, G., J. Vormbrock, T. Butz, M. Christ, H.-J. Trappe, and A. Meissner. Different effect of exercise on left ventricular diastolic time and interventricular dyssynchrony in heart failure patients with and without left bundle branch block. *Int. J. Med. Sci.* 5:333–340, 2008.
- ⁵⁵Powell, A. J., S. E. Maier, T. Chung, and T. Geva. Phase-velocity cine magnetic resonance imaging measurement of pulsatile blood flow in children and young adults: in vitro and in vivo validation. *Pediatr. Cardiol.* 21:104–110, 2000.
- ⁵⁶Raffel, M., C. Willert, and J. Kompenhans. Particle Image Velocimetry. Berlin, Heidelberg, Germany: Springer-Verlag, 1998.
- ⁵⁷Raguin, L. G., S. L. Honecker, and J. G. Georgiadis. MRI velocimetry in microchannel networks. In: 3rd IEEE/EMBS Special Topic Conference on Microtechnology in Medicine and Biology, 2005, pp. 319–322.
- ⁵⁸Schenkel, T., M. Malve, M. Reik, M. Markl, B. Jung, and H. Oertel. MRI-based CFD analysis of flow in a human left ventricle: methodology and application to a healthy heart. *Ann. Biomed. Eng.* 37(3):503–515, 2009.
- ⁵⁹Shaw, G. R., and P. Savard. On the detection of QRS variations in the ECG. *IEEE Trans. Bio-Med. Eng.* 42(7):736–741, 1995.
- ⁶⁰Stallmann, F. W., and H. V. Pipberger. Automatic recognition of electrocardiographic waves by digital computer. *Circ. Res.* 9:1138–1143, 1961.
- ⁶¹Tang, A., D. Kacher, E. Lam, M. Brodsky, F. Jolesz, and E. Yang. Multi-modal imaging: simultaneous MRI and ultrasound imaging for carotid arteries visualization. In: Proceedings of the 29th Annual International Conference of the IEEE (EMBS 2007), Lyon, France, 2007, pp. 2603–2606.
- ⁶²Teo, K. S. L., K. Roberts-Thomson, and S. G. Worthley. Utility of intravascular ultrasound in the diagnosis of ambiguous calcific left main stenoses. *J. Invasive Cardiol.* 16:385, 2004.
- ⁶³Tetsuya, M. ECG gating in cardiac MRI. *Jpn. J. Magnet. Reson. Med.* 23(4):120–130, 2003.
- ⁶⁴Thompson, R. B., and E. R. McVeigh. Flow-gated phase-contrast MRI using radial acquisitions. *Magnet. Reson. Med.* 52(3):598–604, 2004.
- ⁶⁵Trahanias, P. E. An approach to QRS complex detection using mathematical morphology. *IEEE Trans. Bio-Med. Eng.* 40(2):201–205, 1993.
- ⁶⁶Uterhinninghofen, R., S. Ley, J. Zaporozhan, G. Szabö, and R. Dillmann. A versatile tool for flow analysis in 3D-phase-contrast magnetic resonance imaging. *Int. J. Comput. Assist. Radiol. Surg.* 1(1):107–117, 2006.
- ⁶⁷Vasan, R. S., M. G. Larson, E. J. Benjamin, J. C. Evans, C. K. Reiss, and D. Levy. Congestive heart failure in subjects with normal versus reduced left ventricular ejection fraction. *J. Am. Coll. Cardiol.* 33:1948–1955, 1999.
- ⁶⁸Wahle, A., J. J. Lopezd, M. E. Olszewskia, S. C. Vigmostadb, K. B. Chandran, J. D. Rossenc, and M. Sonkaa. Plaque

- development, vessel curvature, and wall shear stress in coronary arteries assessed by X-ray angiography and intravascular ultrasound. *Med. Image Anal.* 10(4):615–631, 2006.
- ⁶⁹Webb, G., and M. A. Gatzoulis. Atrial septal defects in the adult—recent progress and overview. *Circulation* 114:1645–1653, 2006.
- ⁷⁰Wigstrom, L., L. Sjoqvist, and B. Wranne. Temporally resolved 3D phase contrast imaging. *Magnet. Reson. Med.* 36:800–803, 1996.
- ⁷¹Wolbarst, A. B. Looking Within How X-ray, CT, MRI, Ultrasound, and Other Medical Images are Created, and How They Help Physicians Save Lives. USA: University of California Press, 1999.
- ⁷²Wong, K. K. L., R. M. Kelso, S. G. Worthley, P. Sanders, J. Mazumdar, and D. Abbott. Medical imaging and processing methods for cardiac flow reconstruction. *J. Mech. Med. Biol.* 9(1):1–20, 2009.
- ⁷³Wong, K. K. L., R. M. Kelso, S. G. Worthley, P. Sanders, J. Mazumdar, and D. Abbott. Theory and validation of magnetic resonance fluid motion estimation using intensity flow data. *PLoS ONE* 4(3):e4747, 2009.
- ⁷⁴Yamashita, S., H. Isoda, M. Hirano, H. Takeda, S. Inagawa, Y. Takehara, M. T. Alley, M. Markl, N. J. Pelc, and H. Sakahara. Visualization of hemodynamics in intracranial arteries using time-resolved three-dimensional phase-contrast MRI. *J. Magn. Reson. Imag.* 25:473–478, 2007.
- ⁷⁵Yang, G. Z., R. H. Mohiaddin, P. J. Kilner, and D. N. Firmin. Vortical flow feature recognition: a topological study of in-vivo flow patterns using MR velocity mapping. *J. Comput. Assist. Tomogr.* 22:577–586, 1998.
- ⁷⁶Zhao, S. Z., P. Papathanasopoulou, Q. Long, I. Marshall, and X. Y. Xu. Comparative study of magnetic resonance imaging and image-based computational fluid dynamics for quantification of pulsatile flow in a carotid bifurcation phantom. *Ann. Biomed. Eng.* 31(8):962–971, 2003.
- ⁷⁷Zile, M. R., and D. L. Brutsaert. New concepts in diastolic dysfunction and diastolic heart failure: Part I. *Circulation* 105:1387–1393, 2002.